Journal of Molecular Catalysis A: Chemical 356 (2012) 53–60

Contents lists available at SciVerse ScienceDirect

Journal of Molecular Catalysis A: Chemical

journal homepage: www.elsevier.com/locate/molcata

Low-temperature synthesis of CdS/TiO_2 composite photocatalysts: Influence of synthetic procedure on photocatalytic activity under visible light

Jian-wen Shi [a,b], Xiaoxia Yan [b], Hao-Jie Cui [a], Xu Zong [b], Ming-Lai Fu [a], Shaohua Chen [a,*], Lianzhou Wang [b,**]

[a] Key Laboratory of Urban Environment and Health, Institute of Urban Environment, Chinese Academy of Sciences, No. 1799, Jimei Road, Xiamen, Fujian 361021, China
[b] ARC Centre of Excellence for Functional Nanomaterials, School of Chemical Engineering, The University of Queensland, QLD 4072, Australia

ARTICLE INFO

Article history:
Received 3 November 2011
Received in revised form
20 December 2011
Accepted 1 January 2012
Available online 8 January 2012

Keywords:
CdS/TiO_2
Hydrothermal synthesis
Visible light
Photocatalytic activity

ABSTRACT

CdS/TiO_2 composites were successfully prepared by hydrothermal treatment at a considerably low temperature (180 °C). The effects of four different synthetic procedures on the microstructures of CdS/TiO_2 composites, such as morphology, crystal structure, porous property and optical response, were investigated in detail. It was found that CdS/TiO_2 composites consisted of anatase TiO_2 and cubic phase CdS. The hydrothermal treatment of mixed reactant-containing solution improved the crystallinity of both CdS and TiO_2. The abundant pores in catalyst particles formed by CO_2 gas bubbles due to hydrothermal decomposition of the urea molecules increased the specific surface area and pore volume of the catalysts. Meanwhile, the absorption edges of CdS/TiO_2 samples were drastically extended to around 550 nm. The photocatalytic activities of these prepared samples were evaluated by the photocatalytic decoloration of rhodamine B and methyl orange under visible light irradiation ($\lambda > 420$ nm), respectively. The sample prepared by hydrothermal reaction with CdS and TiO_2 in the molar ratio of 0.25:1 showed the highest photocatalytic activity under visible light irradiation among all samples in this work, which could be attributed to the synergic effects of some factors, such as the excellent crystallinity, high specific surface area, large pore volume and strong absorption in the visible light region. Based on the results of the present study, a reasonable mechanism of photocatalysis on CdS/TiO_2 composite under visible light was proposed.

1. Introduction

Textile and other dye-related industries produce various organic pollutants. If these pollutants are discharged into the surrounding environment without any further treatment, it not only introduces color to water but also causes extensive toxicity to the aquatic and other forms of lives because they can be reduced to potential carcinogenic substances under anaerobic conditions [1–3]. In order to eliminate the potential danger of these recalcitrant organic dyes, many technologies, such as flocculation [4], adsorption [5], ultrafiltration [6], reverse osmosis [7] and extraction [8], have been developed to treat these pollutants. However these techniques are nondestructive since they simply transfer the pollutant from one phase to another [9]. Therefore, it is very important to develop new methods of decomposing these organic dyes completely.

Over the past few years, several advanced oxidation processes, such as ultraviolet light (UV), hydrogen peroxide, ozonation, Fenton, photocatalysis and the combination of these technologies, have been proposed as alternative routes for water purification [10–13]. Among these technologies, heterogeneous photocatalysis seems to be the most attractive method to decompose harmful organic pollutants to final non-toxic products [14,15]. Titanium dioxide (TiO_2) is the most popular photocatalyst used in heterogeneous photocatalysis for its excellent properties, such as high stability, low cost and environmental friendliness [16]. However, a major drawback of TiO_2 is that only UV in the solar spectrum (about 3–5%) can be utilized to initiate the photocatalytic redox processes because of the large band gap of anatase TiO_2 (3.2 eV) [17]. Another major limiting factor is the high rate of recombination of the photogenerated electron–hole pairs, which results in a poor rate of electrons (and holes) that reaches the interface between photocatalyst and liquid, where the photocatalytic degradation takes place [18]. These two factors strongly inhibit the large-scale application of the naked TiO_2 in solar-driven water purification.

The above problems can be solved, in part, if TiO_2 is coupled by a smaller band gap semiconductor with a higher conduction band (CB) than that of TiO_2 [19]. Firstly, semiconductor with narrow band gap can improve the efficiency of solar energy absorption. Secondly, the electron generated in the CB of the narrow band gap semiconductor can be injected into that of TiO_2, which can therefore reduce the recombination probability of electrons and holes

* Corresponding author. Tel.: +86 592 6190995; fax: +86 592 6190977.
** Corresponding author. Tel.: +61 7 336 54218; fax: +61 7 336 54199.
E-mail addresses: shchen@iue.ac.cn (S. Chen), l.wang@uq.edu.au (L. Wang).

1381-1169/$ – see front matter © 2012 Elsevier B.V. All rights reserved.
doi:10.1016/j.molcata.2012.01.001

by keeping oxidation and reduction processes in different reaction sites [20]. For instance, TiO_2 coupled by CdS have been extensively investigated in photoelectrochemistry and water splitting systems due to the suitable band gap (2.4 eV) and excellent optical property of CdS [21–24].

To date, CdS/TiO_2 composites with different structures, such as nanoparticle [25], nanorod [26], nanotube [22], film [27] and core–shell [28] have been prepared successfully. Moreover, various synthetic methods, such as reverse micellar route [28], precipitation [29], chemical bath deposition [30], dipping and deposition technique [21] and other unnamed methods [31,32] have been used. Most of these methods are performed at high temperatures, typically from 300 to 600 °C, which leads to the increase of the crystallite size and the decrease of the specific surface area, and thus hampers the enhancement of photocatalytic activity [33]. Furthermore, CdS in CdS/TiO_2 composite can be oxidized during thermal treatment for the crystallinity of TiO_2 [31]. Therefore, it is highly desirable to synthesize CdS/TiO_2 composite with high visible-light photocatalytic activity by low-temperature method. However, generally, the low-temperature preparation of photocatalyst brings new problem: poor crystallinity, which is detrimental to photocatalytic activity, so the preparation of CdS/TiO_2 composite by low-temperature method (below 200 °C) has been rarely reported up to now. To our knowledge, only two papers mentioned the synthesis of CdS/TiO_2 composite at low temperature in the literature [34,35]. Wu et al. [34] prepared CdS coupled with TiO_2 nanocrystal by a microemulsion-mediated solvothermal method at a relatively low temperature (200 °C); however, long-time solvothermal treatment (at least 12 h) was required for improving the crystallinity of the two components. Ghows and Entezari [35] synthesized CdS/TiO_2 nanocrystal with core–shell structure at low temperature by micro-emulsion under ultrasound, but the crystallinity of products was still unsatisfactory. Furthermore, the influences of synthetic conditions on the microstructures and photocatalytic activity of CdS/TiO_2 composite under visible light have not been reported yet.

In the present work, CdS/TiO_2 composites with better crystallinity were successfully synthesized with a hydrothermal reaction at 180 °C for 6 h. The effects of different synthetic procedures on the microstructures of CdS/TiO_2 composites, such as morphology, crystal structure, porosity and optical response, were investigated in detail. Their photocatalytic activities were further evaluated by the photocatalytic decoloration of two kinds of common dyes, rhodamine B (RhB) and methyl orange (MO) under visible light irradiation ($\lambda > 420$ nm), respectively.

2. Experimental

2.1. Synthesis of CdS

0.52 g of $CdCl_2$ and 0.68 g of $Na_2S{\cdot}9H_2O$ were introduced into two beakers containing 10 mL of ethanol and 5 mL of deionized water, respectively. After stirring for 30 min, the sodium sulfide solution was added dropwise into the cadmium chloride solution under magnetic agitation. The resultant mixture was continuously stirred for 60 min at ambient temperature to form an orange floc (marked as A). The floc was centrifuged to obtain solid deposition, which was then re-dispersed, washed, and centrifuged in water and in ethanol for three cycles, respectively. Finally, the as-obtained product was dried at 80 °C for 12 h in an oven, resulting in CdS photocatalyst.

2.2. Synthesis of TiO_2

3.4 mL of titanium (IV) isopropoxide and 4.8 mL of glacial acetic acid were first dissolved in 30 mL of ethanol to form a clear solution, 0.6 g of polyethylene glycol (PEG, molecular weight 2000) and 0.6 g of urea ($CO(NH_2)_2$) were then added to the clear solution under magnetic stirring at 40 °C to form a transparent solution (marked as B). Then, the transparent solution B was transferred into a Teflon-lined stainless steel autoclave with 80 mL capacity. Afterwards, the autoclave was heated at 180 °C for 6 h and then cooled to ambient temperature naturally. The obtained product of the hydrothermal reaction was centrifuged, washed, and re-dispersed in water and in ethanol for three cycles, respectively. Finally, the product was dried at 80 °C for 12 h in an oven, resulting in TiO_2 photocatalyst.

2.3. Synthesis of CdS/TiO_2 composite

2.3.1. Procedure 1

The floc A (prepared by the route described in Section 2.1) was added into the solution B (prepared by the route described in Section 2.2) dropwise at room temperature under magnetic agitation. After stirring for 60 min, a yellow sol of mixed CdS and TiO_2 was formed. The sol was transferred into a Teflon-lined stainless steel autoclave, and the autoclave was sealed and heated at 180 °C for 6 h. After cooling to ambient temperature naturally, the product of the hydrothermal reaction was collected and washed with water and ethanol for three times, respectively. Finally, the product was dried at 80 °C for 12 h in an oven, resulting in CdS/TiO_2 composite. Different ratios of CdS and TiO_2 were obtained by adjusting the dosage of the precursors. The CdS/TiO_2 sample synthesized by this procedure was denoted as S1(*X*), where *X* represented the molar ratio of CdS and TiO_2. For instance, if the molar ratio of CdS and TiO_2 was 0.25:1, the sample was denoted as S1(0.25).

2.3.2. Procedure 2

The sample S2(*X*) was obtained by calcining sample S1(*X*) at 400 °C in air for 2 h. The purpose of heat treatment was to compare the influence of low-temperature synthesis and high-temperature heat treatment on the microstructures and the photocatalytic activities of CdS/TiO_2.

2.3.3. Procedure 3

Procedure 3 was similar with procedure 1, while no hydrothermal treatment was used. The yellow CdS and TiO_2 mixed product was directly collected and washed with water and ethanol. Then, the final product was dried at 80 °C for 12 h in an oven. The sample synthesized according to this procedure was denoted as S3(*X*).

2.3.4. Procedure 4

TiO_2 particles prepared according to the method described in Section 2.2 were dispersed in the orange floc A. Secondly, the obtained mixture was transferred to a Teflon-lined stainless steel autoclave, and the autoclave was then heated at 180 °C for 6 h. After cooling to ambient temperature, the product was centrifuged, washed, and re-dispersed in water and in ethanol for three times, respectively. Finally, the product was dried at 80 °C for 12 h in an oven. The sample synthesized according to this procedure was denoted as S4(*X*).

2.4. Characterizations

Scanning electron microscopy (SEM) images were obtained by a JEOL 6300 (Tokyo, Japan) equipment. The surface elements composition over the desired region of sample were detected by an energy dispersive X-ray spectrometer (EDX) attached to the SEM. Transmission electron microscope (TEM) tests were carried out on a JEM 2100 (JEOL, Japan) equipment. X-ray diffraction (XRD) patterns were recorded on a Rigaku MiniFlex powder diffractometer using cobalt Kα radiation. The nitrogen adsorption measurements were carried out at 77 K using a Micromeritics ASAP 2010, and the pore size distributions and specific surface

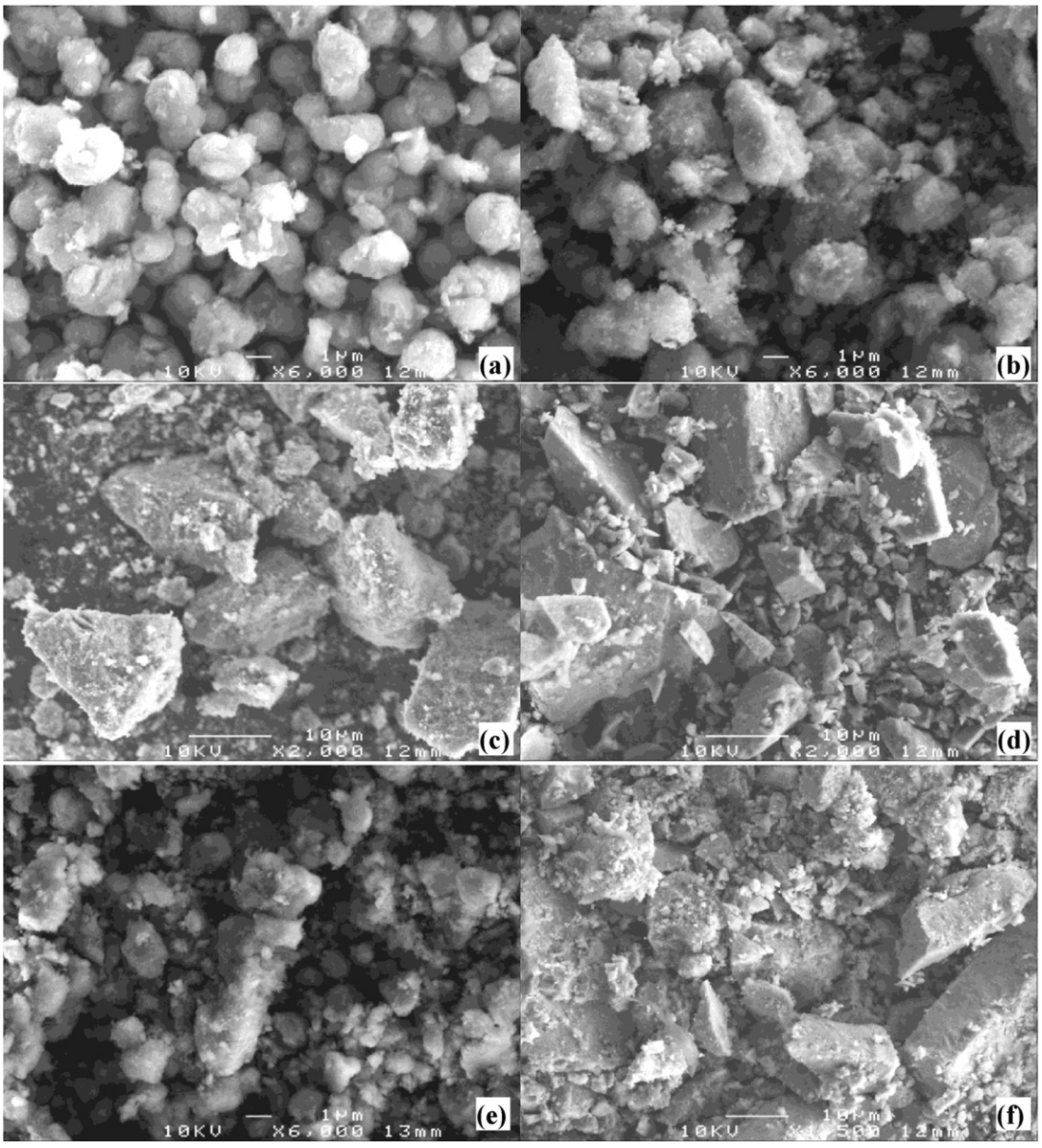

Fig. 1. SEM images of samples: (a) TiO_2; (b) S1(0.25); (c) S2(0.25); (d) S3(0.25); (e) S4(0.25); (f) CdS.

areas were calculated according to the Density Functional Theory (DFT) [36] and the Brunauer–Emmett–Teller (BET) model, respectively. Ultraviolet–visible (UV–vis) absorption spectra of all samples were recorded by a Shimadzu spectrophotometer (UV-2450, Japan) equipped with an integrating sphere, and the baseline correction was done using a calibrated sample of barium sulfate. FTIR spectra of samples were investigated by using a Nicolet FTIR spectrometer (Magna-750) at ambient conditions.

2.5. Experimental procedures of photocatalytic degradation

The photocatalytic experiments were carried out by adding 100 mg of photocatalysts into 100 mL of 20 mg/L dye (RhB or MO) solution. The suspension was ultrasonicated for 30 min, and then stirred for 30 min in dark to obtain the saturated adsorption of dye molecules before illumination. The suspension was irradiated with a 300 W Xe lamp equipped with a 420 nm cut-off glass filter (removing the UV irradiation below 420 nm wavelength). During the irradiation, the suspension was stirred continuously. For comparison, TiO_2, CdS and the commercial Degussa P25 were also examined under the same conditions. At given time interval, 3 mL of suspension was taken out and immediately centrifuged to eliminate the solid particles. The absorbance of the filtrate was measured by a spectrophotometer (UV-2450, Japan) at the maximum absorbance peak (554 nm for RhB and 465 nm for MO). Note that in order to remove the possible organic substance in the samples completely, the samples were directly irradiated under a 300 W Xe lamp in an oxygen atmosphere [37] for 3 h before they were used as photocatalysts (FTIR result, see Fig. A.1) confirmed that the possible organic residues were completely removed).

3. Experimental results and discussion

3.1. Morphology

Fig. 1 shows the SEM images of TiO_2, CdS, and CdS/TiO_2 prepared by four different procedures. It can be observed from Fig. 1a

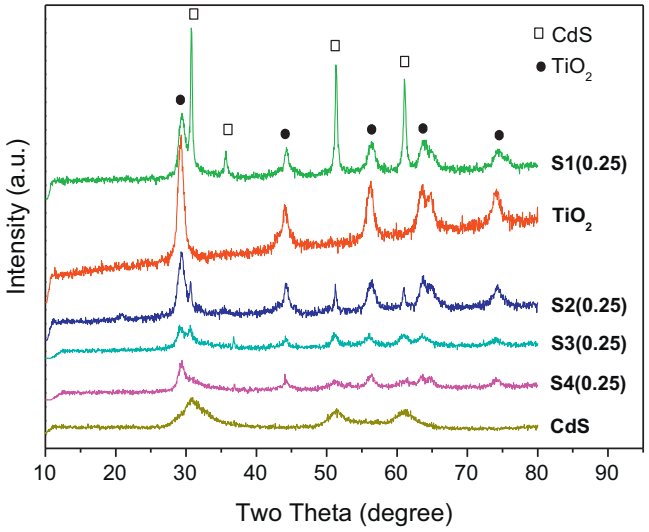

Fig. 2. XRD patterns of the samples.

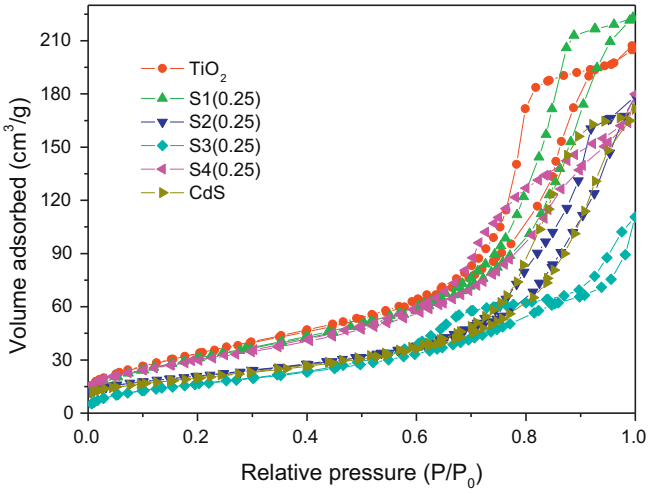

Fig. 3. Nitrogen adsorption–desorption isotherms of the samples.

that TiO_2 prepared by hydrothermal reaction presented slippery spherical morphology with uniform diameter of about 2 μm.

After CdS was introduced, the spherical morphology was changed and the surface of particles became relatively rough (Fig. 1b). Agglomeration happened after CdS/TiO_2 sample was calcined at 400 °C for 2 h, and the sizes of some particles were increased to about 10 μm (Fig. 1c). When CdS/TiO_2 sample was prepared according to procedure 3, agglomerates with irregular morphology and size ranging from few micrometers up to tens of micrometer are observed in Fig. 1d. In order to obtain more information of the big chunks in Fig. 1d, a higher resolution SEM with EDX is provided in Fig. A.2, and the result of EDX confirmed the surface of S3(0.25) contained titanium, oxygen, cadmium, sulfur, and a little adventitious carbon, as it was expected. The morphology of CdS shown in Fig. 1f looked exactly similar to that of CdS/TiO_2 sample displayed in Fig. 1d because no hydrothermal process was applied during the synthesis of the two samples. In Fig. 1e, we can observe that TiO_2 still maintained spherical morphologies, and CdS particles were deposited.

3.2. Crystal phase composition

To determine the crystal phase composition of the prepared samples, XRD measurements were carried out (Fig. 2). It can be observed that all CdS/TiO_2 samples consisted of two kinds of crystal phases: anatase TiO_2 and cubic CdS [34]. No extra peaks except for anatase phase were observed in the XRD pattern of TiO_2 sample, and no extra peaks except for cubic CdS were found in CdS sample. In comparison with other CdS/TiO_2 samples and the results of Wu et al. [34] and Ghows and Entezari [35], CdS in sample S1(0.25) presented a better crystallinity with sharper and stronger XRD peaks. Compared the XRD pattern of S1(0.25) with that of S2(0.25), it can be concluded the crystallinity of anatase TiO_2 was not improved by the heat treatment at 400 °C in air; on the contrary, the crystallinity of cubic CdS was reduced, which may be due to the partial oxidation of CdS in CdS/TiO_2 composite during thermal treatment. The crystallinity of anatase TiO_2 and that of cubic CdS in sample S3(0.25) both were not good due to the absence of hydrothermal process. The weak XRD peaks of anatase TiO_2 in S4(0.25), which is expected to be as strong as TiO_2 sample, were caused by the coverage of CdS with poor crystallinity, like what can be observed in Fig. 1e. From the above experimental results, it can be inferred that hydrothermal process is the necessary condition in the current work to obtain good crystallinity. With the hydrothermal treatment, the crystallinity of both CdS and TiO_2 was increased.

As we well know, crystallinity plays a very important role in the photocatalytic activity of TiO_2. Better crystallinity can decrease the crystal defect, which is supposed to be the recombination center of photo-generated electrons and holes [38–43]. Therefore, better crystallinity can improve the photocatalytic activity of TiO_2 [44–47]. The charge transfer in CdS/TiO_2 photocatalyst is different from that in TiO_2. In CdS/TiO_2 photocatalyst, the photogenerated electrons in CdS are transferred to the TiO_2 particles while the holes remain in the CdS particle, which can lead to efficient charge separation, and reduce the recombination of electrons and holes [34,48]. However, electron–hole recombination in the bulk of CdS is still difficult to avoid. Well crystallized CdS might facilitate the transfer of photo-generated electrons from bulk to surface and thus inhibit their recombination with photo-generated holes, leading to the enhancement of quantum efficiency.

The crystal size of anatase was estimated based on the full width at half-maximum (FWHM) of the (1 0 1) peak of anatase according to the Scherrer equation shown as follows:

$$D = \frac{K\lambda}{\beta \cos\theta} \quad (1)$$

where K is a constant (shape factor, about 0.89), λ is the X-ray wavelength, β is the FWHM of the diffraction line, and θ is the diffraction angle. The calculated results are shown in Table 1. It can be observed that the average particle sizes of all samples prepared in this work were about 10 nm, implying that the effects of different synthetic procedures on the crystal size of anatase were trivial.

3.3. Nitrogen adsorption–desorption isotherm and porous structure

In order to investigate the porous properties of the as-prepared samples, nitrogen adsorption–desorption isotherms were measured. It can be seen from Fig. 3 that the isotherms of all samples revealed a typical type IV sorption behavior with the hysteresis loops, representing the predominant mesoporous structure characteristic according to the classification of IUPAC [49–51]. The pore size distributions of samples are expressed in Fig. 4. TiO_2 presented a very uniform pore diameter with a sharp maximum at 40 nm. These pores were formed by the accumulation of nanoparticles (see the TEM images shown in Fig. A.3), which created a large number of inter-nanoparticle voids in structure to increase the specific surface area and total pore volume of samples. CO_2 bubbles

Table 1
Calculation results of some parameters.

Sample	S_{BET} (m^2/g)	Total pore volume (cm^3/g)	Crystal size of anatase TiO_2 (nm)	Band gap energy (eV)
P25	53.3	0.105	24.7	3.04
TiO_2	128.0	0.297	10.6	3.17
S1(0.25)	117.7	0.331	11.1	2.14
S2(0.25)	74.7	0.252	14.2	2.29
S3(0.25)	63.6	0.142	9.9	2.06
S4(0.25)	109.2	0.239	12.3	2.19
CdS	71.6	0.251	NA	2.03

due to hydrothermal decomposition of the urea molecules according to the reaction equation $CO(NH_2)_2 + 3H_2O = 2NH_3{\cdot}H_2O + CO_2$ [52], played a role to avoid the accumulation of nanoparticles too dense. Moreover, the dissolution of PEG molecules, as a structure-directing agent [52,53], during the repetitious washing by water and ethanol from the formed particles was the other reason of porous structure formation in the sample. The diameters of pores formed in S3(0.25) were mainly in 20–30 nm. Some larger pores, even macropores (50–60 nm), were formed in the other samples. Compared with S1(0.25), more macroporous structure (60–90 nm) appeared in S2(0.25), and the quantity of smaller pores decreased, which indicated that some pores collapsed during calcination [54,55].

Table 1 shows the specific surface area (S_{BET}) and total pore volume of all samples. It can be seen that these samples (TiO_2, S1(0.25) and S4(0.25)) prepared by hydrothermal reaction possessed larger S_{BET} and total pore volume than those samples (S3(0.25) and CdS) without hydrothermal process. There was a significant decrease in the S_{BET} of S2(0.25) due to the collapses of some pores during heat treatment.

Specific surface area and total pore volume play important roles in determining the activity of photocatalyst because heterogeneous photocatalysis is a surface-based phenomenon [56–58]. Sample with larger specific surface area and total pore volume can pre-adsorb more organic molecules on the surface of sample, which helps to reduce the recombination of photogenerated electron and hole, and improves the efficiency of photocatalytic degradation [59]. Furthermore, the surface area can be correlated with the number of effective active sites. The increase of surface area means the increase of active sites on which organic molecules and intermediate products are adsorbed [60,61]. Therefore, the larger S_{BET} of S1(0.25) indicates the resultant CdS/TiO_2 composite could be very promising in the application of photocatalytic degradation of organic pollutants.

3.4. Optical response

Fig. 5 shows the UV–vis absorption spectra of all samples, together with those of P25, TiO_2 and CdS as comparison. The CdS/TiO_2 samples exhibited strong absorption in the visible region. In comparison with P25 and TiO_2, the absorption edge of CdS/TiO_2 was drastically extended to around 550 nm due to the addition of a small portion of CdS. Furthermore, the spectra of CdS/TiO_2 photocatalysts showed a combination of the two spectra from CdS and TiO_2, respectively. Compared with other CdS/TiO_2 samples, the absorption intensity of sample S2(0.25) in the visible region decreased by a third due to heat treatment. The absorption onset was determined by linear extrapolation from the inflection point of the curve to the baseline [34,62], and the band gap energy of samples was estimated by the following formula [63–65] and the results are shown in Table 1.

$$E_g = \frac{1240}{\lambda_{onset}} \quad (2)$$

where E_g is the band gap energy and λ_{onset} is the absorption onset. It can be observed that the band gap of CdS/TiO_2 photocatalysts decreased significantly in comparison with P25 and TiO_2, indicating that CdS/TiO_2 samples can be excited by visible light. As is known, the absorption of visible light is the basis of the photocatalytic activity under visible light. The optical absorption data implies that the CdS/TiO_2 compounds synthesized in this work could be promising in visible light photocatalysis [66].

3.5. Photocatalytic activity

The cation dye of RhB is one of the most commonly used xanthenes dyes for textile industry and is well-known for its good stability [67]. RhB has been widely chosen as a model pollutant to evaluate the photocatalytic activity of TiO_2 or other

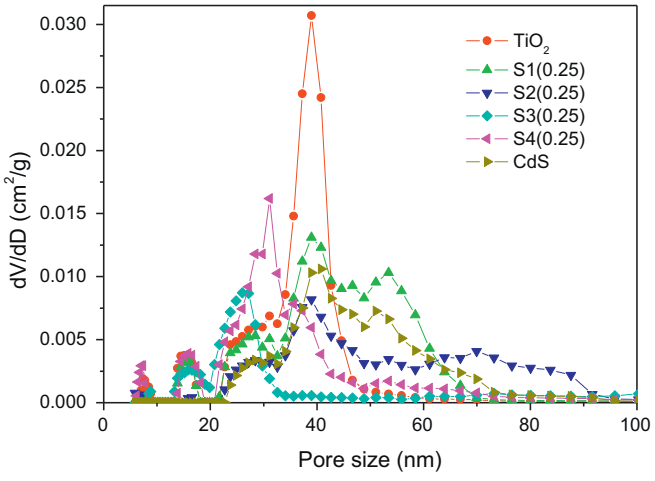

Fig. 4. Pore size distributions of the samples obtained from the desorption branch.

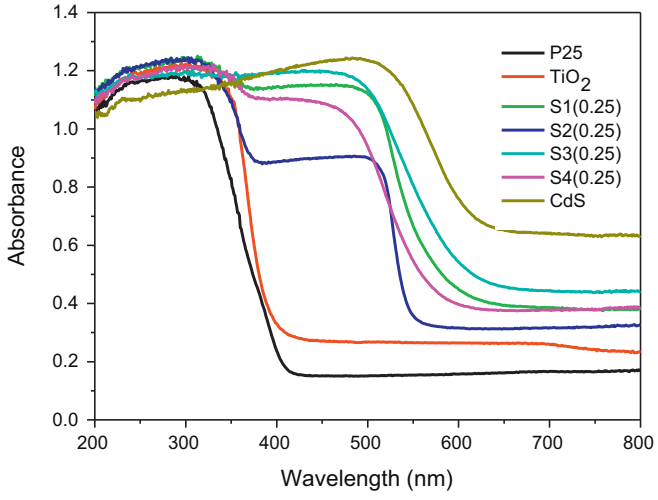

Fig. 5. UV–vis spectra of the samples.

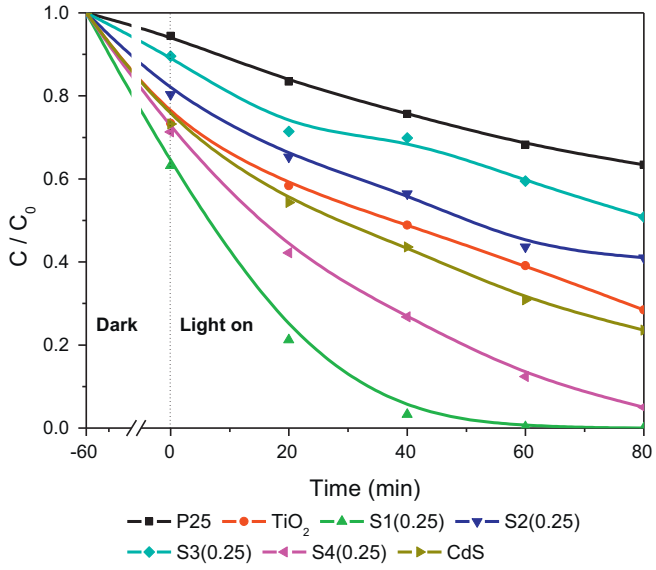

Fig. 6. Decoloration curves of RhB solution by the samples under visible light irradiation (λ > 420 nm).

photocatalysts [68,69]. In the current work, the photocatalytic activities of CdS/TiO_2 samples were evaluated by the decoloration of RhB solution without investigating the degradation intermediates in detail. For comparison, the photocatalytic activities of P25, TiO_2 and CdS were also tested. The discoloration of RhB solution versus photocatalytic time under visible light irradiation (λ > 420 nm) is shown in Fig. 6. Although P25 and TiO_2 could not respond to visible light, RhB can be decomposed slowly under visible light irradiation in the presence of P25 or TiO_2, which can be attributed to the photosensitized capability of RhB. S1(0.25) presented the optimal efficiency of photocatalytic decoloration among all samples.

MO is a very stable azo dye and has been used as a probe for photocatalytic decolorization [70,71]. In order to further confirm the photocatalytic activities of these samples under visible light irradiation, the photocatalytic decoloration of MO solution by these samples was also carried out under the same conditions and the results are shown in Fig. 7. Compared with RhB, MO solution was

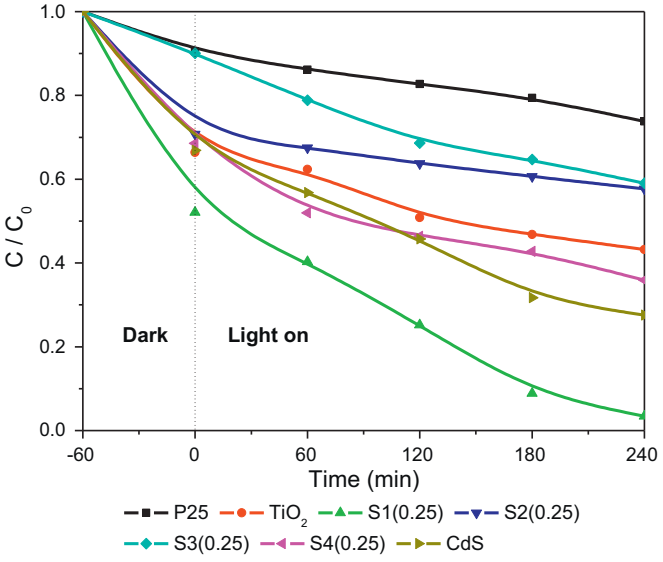

Fig. 7. Decoloration curves of MO solution by the samples under visible light irradiation (λ > 420 nm).

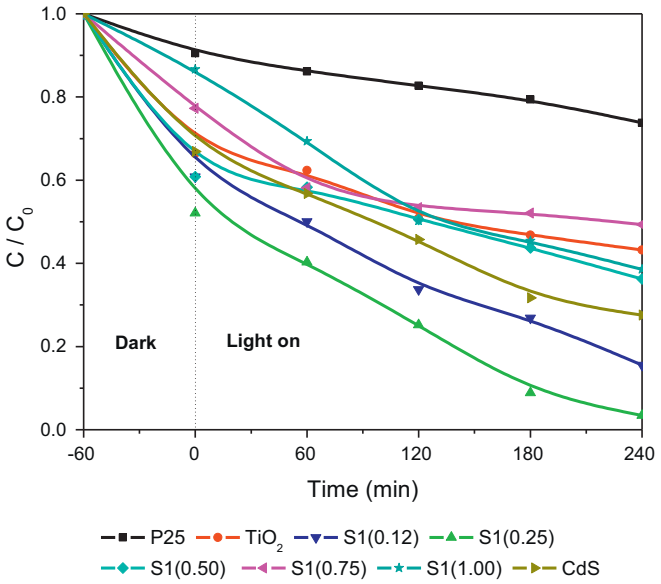

Fig. 8. Decoloration curves of MO solution by the CdS/TiO_2 samples with different ratio of CdS and TiO_2 under visible light irradiation (λ > 420 nm).

more difficult to be decolorized because of its stabilization and low photosensitized property [72]. However, as shown in Fig. 7, the CdS/TiO_2 samples presented higher photocatalytic activity and the MO solution can be decolorized under visible light irradiation. Similarly, the sample S1(0.25) showed the highest activity among all samples.

In addition, in order to investigate the optimal molar ratio of CdS and TiO_2, we prepared CdS/TiO_2 samples with different molar ratio of CdS and TiO_2 according to procedure 1 and evaluated their photocatalytic activities by the photocatalytic decoloration of MO under the same conditions. It can be observed from Fig. 8 that the S1(0.25) sample showed the highest activity among all CdS/TiO_2 samples, indicating that the optimal molar ratio of CdS and TiO_2 was 0.25:1 for the CdS/TiO_2 photocatalysts synthesized by procedure 1.

As described above, both the decoloration of the RhB and MO over the photocatalysts prepared in this work show similar trends: the sample S1(0.25) possesses the highest photocatalytic activity under visible light irradiation among all samples, which can be attributed to the synergic effects of a number of factors, such as the excellent crystallinity, high specific surface area (117.7 m^2/g), large pore volume (0.331 cm^3/g) and strong absorption in the visible light region. Furthermore, the latter is probably the most important factor as the absorption of visible light is the basis of the photocatalytic activity under visible light. In addition, the intimate contact between CdS and TiO_2, which was confirmed by the HRTEM of S1(0.25) (see Fig. A.4), may be the other reason why S1(0.25) possessed the highest photocatalytic activity. The intimate contact between CdS and TiO_2 favors the formation of junctions between the two components and, as a result, improves the charge separation and therefore the photocatalytic activity [73].

3.6. Proposed mechanism

The mechanisms of visible light-induced photocatalytic activity of the CdS/TiO_2 have been discussed in early reports [34,48,66,74,75], and the photocatalytic degradation mechanisms of RhB and MO on TiO_2 or other photocatalysts have also been proposed [76–81]. Based on previous publications and our experimental results, we attempt to propose the reaction mechanism for the degradation of dyes on CdS/TiO_2 under visible light irradiation as follows, which is also schematically summarized in Fig. 9.

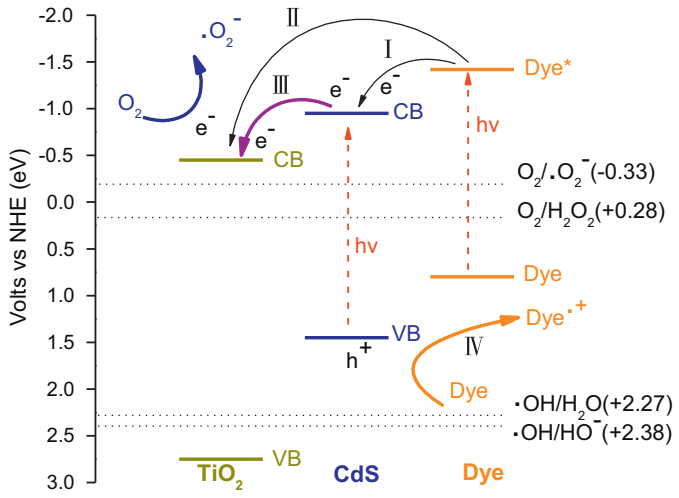

Fig. 9. Photocatalytic mechanism on the CdS/TiO_2 photocatalyst under visible light irradiation.

Firstly, some dye molecules adsorbed on photocatalyst are stimulated to the excited state by absorbing visible light due to the sensitization mechanism (Eq. (3)). Secondly, an electron will be injected into the CB of CdS or TiO_2 from the excited dye molecule (Route I or II shown in Fig. 9), and at the same time, the dye molecule is converted to the cationic dye radical (Eqs. (4) and (5)). Meanwhile, CdS is readily excited under visible light irradiation to yield electron–hole pairs due to its narrow band gap (~2.4 eV) (Eq. (6)). The electrons existed in the CB of CdS, are quickly transferred to the CB of TiO_2 because the CB of CdS is −0.5 eV is more negative than that of TiO_2 (Route III, Eq. (7)). Subsequently, because the E_{CB} of TiO_2 (−0.45 V vs. NHE) is more negative than $E(O_2/{}^{\bullet}O_2^-)$ (−0.33 V vs. NHE) and $E(O_2/H_2O_2)$ (+0.28 V vs. NHE), the electrons existed in the TiO_2 CB can be scavenged by molecular oxygen to produce the superoxide radical anion ${}^{\bullet}O_2^-$ (Eq. (8)) and hydrogen peroxide H_2O_2 (Eq. (9)). These newly formed intermediates can inter-react to produce hydroxyl radical OH• (Eq. (10)). Finally, dye molecule is oxidized by these oxidants and is mineralized into final products step by step (Eq. (11)). Moreover, because the E_{VB} of CdS (1.45 V) is more negative than $E({}^{\bullet}OH/OH^-)$ (2.38 V vs. NHE) and $E({}^{\bullet}OH/H_2O)$ (2.27 V vs. NHE), the photo-generated hole formed in the VB of CdS cannot oxidize hydroxyl groups and H_2O molecule to produce hydroxyl radicals, but can oxidize dye molecules to reactive intermediates, and further to final products (Route IV, Eq. (12)). With regard to the photo-corrosion of CdS, an approach is still pursuing and will be discussed in our next work.

$$\mathrm{Dye_{ads} + h\nu \rightarrow Dye_{ads}{}^{*}} \quad (3)$$

$$\mathrm{Dye_{ads}{}^{*} + CdS/TiO_2 \rightarrow Dye_{ads}{}^{\bullet+} + CdS(e^-)/TiO_2} \quad (4)$$

$$\mathrm{Dye_{ads}{}^{*} + CdS/TiO_2 \rightarrow Dye_{ads}{}^{\bullet+} + CdS/TiO_2(e^-)} \quad (5)$$

$$\mathrm{CdS/TiO_2 + h\nu \rightarrow CdS(e^- + h^+)/TiO_2} \quad (6)$$

$$\mathrm{CdS(e^- + h^+)/TiO_2 \rightarrow CdS(h^+)/TiO_2(e^-)} \quad (7)$$

$$\mathrm{CdS(h^+)/TiO_2(e^-) + O_2 \rightarrow CdS(h^+)/TiO_2 + {}^{\bullet}O_2^-} \quad (8)$$

$$\mathrm{CdS(h^+)/TiO_2(e^-) + O_2 + H^+ \rightarrow CdS(h^+)/TiO_2 + H_2O_2} \quad (9)$$

$$\mathrm{H_2O_2 + {}^{\bullet}O_2^- \rightarrow OH^{\bullet} + OH^- + O_2} \quad (10)$$

$$\mathrm{Dye + {}^{\bullet}O_2^- (or\ H_2O_2\ or\ OH^{\bullet}) \rightarrow PRODUCTS} \quad (11)$$

$$\mathrm{CdS(h^+)/TiO_2 + Dye_{ads} \rightarrow CdS/TiO_2 + Dye_{ads}{}^{\bullet+}} \rightarrow \mathrm{CdS/TiO_2 + PRODUCTS} \quad (12)$$

4. Conclusions

In the present work, the CdS/TiO_2 composites with better crystallinity were successfully synthesized by a mild hydrothermal reaction at 180 °C for 6 h. The effects of synthetic procedures on the microstructures and photocatalytic activities of CdS/TiO_2 composites under visible light irradiation were investigated in detail. From the above experimental results and discussion, it was revealed that CdS/TiO_2 composites consisted of anatase TiO_2 and cubic phase CdS. The hydrothermal treatment of CdS and TiO_2 mixed sol improved the crystallinity of both CdS and TiO_2. CO_2 gas bubbles due to hydrothermal decomposition of the urea molecules created abundant pores in the photocatalyst particles, which in turn increased the specific surface area and pore volume of catalyst. In comparison with P25 and TiO_2, the absorption edge of CdS/TiO_2 was drastically extended to around 550 nm due to the addition of a small portion of CdS. The sample S1(0.25) showed the optimized photocatalytic activity under visible light irradiation among all samples, which can be attributed to the synergic effects of some factors, such as the excellent crystallinity, high specific surface area, large pore volume and strong absorption in the visible light region. The photocatalytic mechanism in decoloring model dye compounds was proposed to elucidate the feasibility of such new heterostructured composite photocatalysts, which may shed light on the material design for more efficient visible light photocatalysis.

Acknowledgments

This work was sponsored by the Australia Research Council through its DPs and Centre programs, the Key Program in the Regional Science and Technology of Fujian Province (No. 2009H4006), the Natural Science Foundation of Fujian Province (No. 2010J05036), and the Opening Project of State Key Laboratory of High Performance Ceramics and Superfine Microstructure (No. SKL201107SIC). The authors gratefully thank anonymous reviewers for their insightful comments and valuable suggestions.

Appendix A. Supplementary data

Supplementary data associated with this article can be found, in the online version, at doi:10.1016/j.molcata.2012.01.001.

References

[1] I.M. Banat, P. Nigam, D. Singh, R. Marchant, Bioresour. Technol. 58 (1996) 217–227.
[2] F.P. van der Zee, S. Villaverde, Water Res. 39 (2005) 1425–1440.
[3] S.M. Joshi, S.A. Inamdar, A.A. Telke, D.P. Tamboli, S.P. Govindwar, Int. Biodeter. Biodegr. 64 (2010) 622–628.
[4] L. Semerjian, G.M. Ayoub, Adv. Environ. Res. 7 (2003) 389–403.
[5] G. Crini, Bioresour. Technol. 97 (2006) 1061–1085.
[6] H. Huang, K. Schwab, J.G. Jacangelo, Environ. Sci. Technol. 43 (2009) 3011–3019.
[7] C.Y. Tang, Q.S. Fu, A.P. Robertson, C.S. Criddle, J.O. Leckie, Environ. Sci. Technol. 40 (2006) 7343–7349.
[8] G. Muthuraman, T.T. Teng, C.P. Leh, I. Norli, J. Hazard. Mater. 163 (2009) 363–369.
[9] F. Kiriakidou, D.I. Kondarides, X.E. Verykios, Catal. Today 54 (1999) 119–130.
[10] I. Oller, S. Malato, J.A. Sánchez-Pérez, Sci. Total Environ. 409 (2011) 4141–4166.
[11] A.B. Alvares, C. Diaper, S.A. Parsons, Environ. Technol. 22 (2001) 409–427.
[12] I. Keisuke, E.M. Gamal, J. Environ. Eng. Sci. 5 (2006) 81–135.
[13] P. Saritha, C. Aparnaa, V. Himabindu, Y. Anjaneyulu, J. Hazard. Mater. 149 (2007) 609–614.
[14] U.I. Gaya, A.H. Abdullah, J. Photochem. Photobiol. C 9 (2008) 1–12.
[15] S. Ahmed, M.G. Rasul, W.N. Martens, R. Brown, M.A. Hashib, Desalination 261 (2010) 3–18.
[16] P. Xu, J. Lu, T. Xu, S. Gao, B. Huang, Y. Dai, J. Phys. Chem. C 114 (2010) 9510–9517.
[17] T. Tachikawa, M. Fujitsuka, T. Majima, J. Phys. Chem. C 111 (2007) 5259–5275.
[18] L. Cui, F. Huang, M. Niu, L. Zeng, J. Xu, Y. Wang, J. Mol. Catal. A 326 (2010) 1–7.
[19] D. Robert, Catal. Today 122 (2007) 20–26.
[20] G. Liu, L. Wang, H.G. Yang, H.-M. Cheng, G.Q. Lu, J. Mater. Chem. 20 (2010) 831–843.

[21] Q. Kang, Q.Z. Lu, S.H. Liu, L.X. Yang, L.F. Wen, S.L. Luo, Q.Y. Cai, Biomaterials 31 (2010) 3317–3326.
[22] J. Bai, J. Li, Y. Liu, B. Zhou, W. Cai, Appl. Catal. B 95 (2010) 408–413.
[23] Q. Zhou, M.-L. Fu, B.-L. Yuan, H.-J. Cui, J.-W. Shi, J. Nanopart. Res. 13 (2011) 6661–6672.
[24] H. Park, W. Choi, M.R. Hoffmann, J. Mater. Chem. 18 (2008) 2379–2385.
[25] T. Hirai, K. Suzuki, I. Komasawa, J. Colloid Interface Sci. 244 (2001) 262–265.
[26] X.-M. Song, J.-M. Wu, M. Yan, Electrochem. Commun. 11 (2009) 2203–2206.
[27] A.L. Stroyuk, S.Y. Kuchmii, M.A. Zhukovskii, N.P. Smirnova, E.M. Glebov, V.P. Grivin, V.F. Plyusnin, Theor. Exp. Chem. 45 (2009) 302–307.
[28] S. Vaidya, A. Patra, A.K. Ganguli, Colloids Surf. A 363 (2010) 130–134.
[29] Y. Bessekhouad, D. Robert, J.V. Weber, J. Photochem. Photobiol. A 163 (2004) 569–580.
[30] H. Wang, Y. Bai, H. Zhang, Z. Zhang, J. Li, L. Guo, J. Phys. Chem. C 114 (2010) 16451–16455.
[31] H. Fujii, M. Ohtaki, K. Eguchi, H. Arai, J. Mol. Catal. A 129 (1998) 61–68.
[32] J.S. Jang, H.G. Kim, P.H. Borse, J.S. Lee, Int. J. Hydrogen Energy 32 (2007) 4786–4791.
[33] Y. Xie, Y. Li, X. Zhao, J. Mol. Catal. A 277 (2007) 119–126.
[34] L. Wu, J.C. Yu, X. Fu, J. Mol. Catal. A 244 (2006) 25–32.
[35] N. Ghows, M.H. Entezari, Ultrason. Sonochem. 18 (2011) 629–634.
[36] J.P. Olivier, M.L. Occelli, J. Phys. Chem. B 105 (2001) 623–629.
[37] L. Wang, T. Sasaki, Y. Ebina, K. Kurashima, M. Watanabe, Chem. Mater. 14 (2002) 4827–4832.
[38] K.Y. Jung, S.B. Park, Korean J. Chem. Eng. 18 (2001) 879–888.
[39] M. Mrowetz, W. Balcerski, A.J. Colussi, M.R. Hoffmann, J. Phys. Chem. B 108 (2004) 17269–17273.
[40] J.G. Yu, J.F. Xiong, B. Cheng, S.W. Liu, Appl. Catal. B 60 (2005) 211–221.
[41] L. Jing, Y. Qu, B. Wang, S. Li, B. Jiang, L. Yang, W. Fu, H. Fu, J. Sun, Sol. Energy Mater. Sol. C 90 (2006) 1773–1787.
[42] J.G. Yu, G.H. Wang, B. Cheng, M.H. Zhou, Appl. Catal. B 69 (2007) 171–180.
[43] H.G. Yu, J.G. Yu, B. Cheng, J. Lin, J. Hazard. Mater. 147 (2007) 581–587.
[44] J. Ovenstone, J. Mater. Sci. 36 (2001) 1325–1329.
[45] H. Kominami, J. Kato, S. Murakami, Y. Ishii, M. Kohno, K. Yabutani, T. Yamamoto, Y. Kera, M. Inoue, T. Inui, B. Ohtani, Catal. Today 84 (2003) 181–189.
[46] J.G. Yu, H.G. Yu, B. Cheng, X.J. Zhao, J.C. Yu, W.K. Ho, J. Phys. Chem. B 107 (2003) 13871–13879.
[47] H. Wang, Y. Wu, B.-Q. Xu, Appl. Catal. B 59 (2005) 139–146.
[48] Y. Bessekhouad, N. Chaoui, M. Trzpit, N. Ghazzal, D. Robert, J.V. Weber, J. Photochem. Photobiol. A 183 (2006) 218–224.
[49] J.C. Yu, L. Zhang, J. Yu, Chem. Mater. 14 (2002) 4647–4653.
[50] T. Sreethawong, Y. Yamada, T. Kobayashi, S. Yoshikawa, J. Mol. Catal. A 241 (2005) 23–32.
[51] Y. Liu, Y. Li, Y.T. Wang, L. Xie, J. Zheng, X.G. Li, J. Hazard. Mater. 150 (2008) 153–157.
[52] Y. Cui, L. Liu, B. Li, X. Zhou, N. Xu, J. Phys. Chem. C 114 (2010) 2434–2439.
[53] B. Guo, Z. Liu, L. Hong, H. Jiang, Surf. Coat. Technol. 198 (2005) 24–29.
[54] J. Yu, H. Yu, B. Cheng, C. Trapalis, J. Mol. Catal. A 249 (2006) 135–142.
[55] G. Li, Z.-Q. Liu, J. Lu, L. Wang, Z. Zhang, Appl. Surf. Sci. 255 (2009) 7323–7328.
[56] L. Zhang, Y.F. Zhu, Y. He, W. Li, H.B. Sun, Appl. Catal. B 40 (2003) 287–292.
[57] S.-C. Jung, S.-J. Kim, N. Imaishi, Y.-I. Cho, Appl. Catal. B 55 (2005) 253–257.
[58] X.F. You, F. Chen, J.L. Zhang, J. Sol–Gel Sci. Technol. 34 (2005) 181–187.
[59] J.-W. Shi, J.-T. Zheng, P. Wu, J. Hazard. Mater. 161 (2009) 416–422.
[60] K.Y. Jung, S.B. Park, M. Anpo, J. Photochem. Photobiol. A 170 (2005) 247–252.
[61] Y. Chen, D.D. Dionysiou, J. Mol. Catal. A 244 (2006) 73–82.
[62] Y.J. Zhang, W. Yan, Y. Pei Wu, Z.H. Wang, Mater. Lett. 62 (2008) 3846–3848.
[63] D.S. Bhatkhande, V.G. Pangarkar, A.A.C.M. Beenackers, J. Chem. Technol. Biotechnol. 77 (2001) 102–116.
[64] K.M. Reddy, S.V. Manorama, A.R. Reddy, Mater. Chem. Phys. 78 (2002) 239–245.
[65] V. Stengl, S. Bakardjieva, N. Murafa, V. Houskova, K. Lang, Micropor. Mesopor. Mater. 110 (2008) 370–378.
[66] E. Ghadiri, N. Taghavinia, H.R. Aghabozorg, A. Iraji zad, Eur. Phys. J. Appl. Phys. 20601 (2010) 50–55.
[67] J.-F. Guo, B. Ma, A. Yin, K. Fan, W.-L. Dai, Appl. Catal. B 101 (2011) 580–586.
[68] N. Barka, S. Qourzal, A. Assabbane, A. Nounah, Y. Ait-Ichou, J. Photochem. Photobiol. A 195 (2008) 346–351.
[69] X. Yang, L. Xu, X. Yu, W. Li, K. Li, M. Huo, Y. Guo, Colloids Surf. A 320 (2008) 61–67.
[70] Y. Li, X. Li, J. Li, J. Yin, Water Res. 40 (2006) 1119–1126.
[71] P. Wang, B. Huang, X. Qin, X. Zhang, Y. Dai, J. Wei, M.-H. Whangbo, Angew. Chem. Int. Ed. 47 (2008) 7931–7933.
[72] G. Yang, Z. Jiang, H. Shi, T. Xiao, Z. Yan, J. Mater. Chem. 20 (2010) 5301–5309.
[73] X. Zong, H. Yan, G. Wu, G. Ma, F. Wen, L. Wang, C. Li, J. Am. Chem. Soc. 130 (2008) 7176–7177.
[74] W. Zhao, Z. Bai, A. Ren, B. Guo, C. Wu, Appl. Surf. Sci. 256 (2010) 3493–3498.
[75] X. Yan, G. Liu, L. Wang, Y. Wang, X. Zhu, J. Zou, G.Q. Lu, J. Mater. Res. 25 (2010) 182–188.
[76] P. Qu, J. Zhao, T. Shen, H. Hidaka, J. Mol. Catal. A 129 (1998) 257–268.
[77] M. Yin, Z. Li, J. Kou, Z. Zou, Environ. Sci. Technol. 43 (2009) 8361–8366.
[78] Z. He, C. Sun, S. Yang, Y. Ding, H. He, Z. Wang, J. Hazard. Mater. 162 (2009) 1477–1486.
[79] Z. Yu, H. Keppner, D. Laub, E. Mielczarski, J. Mielczarski, L. Kiwi-Minsker, A. Renken, J. Kiwi, Appl. Catal. B 79 (2008) 63–71.
[80] S.C. Yan, Z.S. Li, Z.G. Zou, Langmuir 26 (2010) 3894–3901.
[81] W. Zhang, D. Li, M. Sun, Y. Shao, Z. Chen, G. Xiao, X. Fu, J. Solid State Chem. 183 (2010) 2466–2474.